Attenuation Characteristics in Confocal Annular Elliptic Waveguides and Resonators

Julio C. Gutiérrez-Vega, Ramón M. Rodríguez-Dagnino, *Member, IEEE*, and Sabino Chávez-Cerda

Abstract—The perturbation method is used to obtain the attenuation constant and Q-factor of several TEM, TE, and TM modes in confocal annular elliptic waveguides (CAE-Ws) and confocal annular elliptic resonators (CAE-Rs). Normalized attenuation and Q-factor charts are given for a variety of possible combinations of the focal distance and the eccentricities. Comparisons between the first higher mode in a CAE-W and a coaxial waveguide with the same cutoff frequency and cross-sectional propagating area reveals a lower attenuation in elliptic geometry. Consequently, the Q-factor in a CAE-R is 20%–40% greater than a Q factor for a coaxial resonator with the same volume and resonant frequency.

Index Terms—Attenuation constant, confocal annular elliptic waveguides, Mathieu functions, perturbation theory, Q factor, resonators.

I. INTRODUCTION

THE confocal annular elliptic (CAE) structures have found increasing application in the design of several microwave devices, e.g., microstrip antennas, resonators, and coaxial probes [1]–[4]. In particular, the elliptic geometry is becoming more popular, as it allows a better control of the polarization characteristics, and facilitates the design by changing both eccentricity and focal length to tune the parameters of interest. CAE structures have been studied by many authors, the formal solution for the propagating modes in confocal annular elliptic waveguides (CAE-Ws) was presented by King and Wiltse [5], Alhargan and Judah [6] provided charts of cutoff frequencies for confocal annular elliptic resonators (CAE-Rs), analytical solutions for frequencies and mode shapes of acoustic CAE-Rs were obtained by Hong and Kim [7], and more recently, Navarro *et al.* [8] presented a method for analyzing CAE-Ws based on the method of moments. On the other hand, the first work on attenuation in hollow elliptic waveguides dates back to 1938 by Chu [9], where charts for the six lowest modes were given. The results of Chu were revised and corrected by several authors in the early 1970s [10]–[12]. Rengarajan *et al.* [13] proved that the use of the intrinsic impedance at all points on the elliptic surface yields practical results, as long as the

J. C. Gutiérrez-Vega was with the Grupo de Fotónica, Instituto Nacional de Astrofísica, Optica y Electrónica, Puebla 64849, México. He is now with the Instituto Tecnológico y de Estudios Superiores de Monterrey, Monterrey 64849, México (e-mail: jgutierr@campus.mty.itesm.mx).

R. M. Rodríguez-Dagnino is with the Instituto Tecnológico y de Estudios Superiores de Monterrey, Monterrey 64849, México (e-mail: rmrodrig@campus.mty.itesm.mx).

S. Chávez-Cerda is with the Grupo de Fotónica, Instituto Nacional de Astrofísica, Optica y Electrónica, Puebla 72000, México (e-mail: sabino@inaoep.mx).

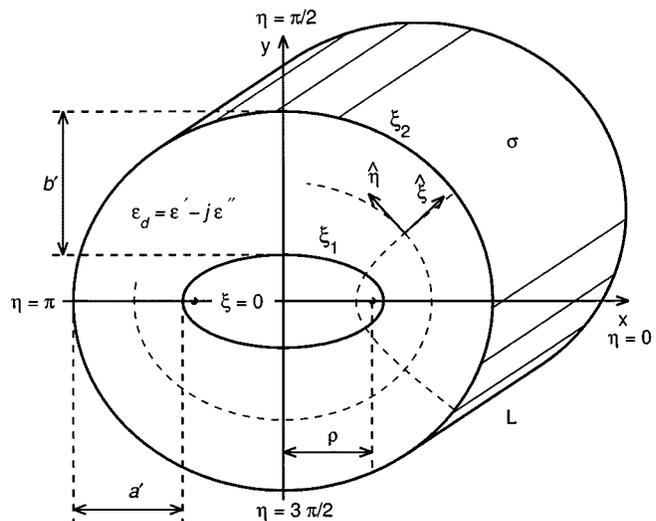Publisher Item Identifier S 0018-9480(02)03016-8.

Fig. 1. Geometry of the CAE structure. The elliptic coordinates are defined by $x = \rho \cosh \xi \cos \eta$ and $y = \rho \sinh \xi \sin \eta$, where $\xi \in [0, \infty)$ is the *radial* coordinate, $\eta \in [0, 2\pi)$ is the *angular* coordinate, and ρ is the focal distance.

radius of curvature is very large compared to the skin depth in the metal.

The purpose of this paper is to present the analysis of the attenuation characteristics of CAE-Ws and CAE-Rs. In particular, we apply first-order perturbation theory to find the theoretical formulas for the attenuation constant of the CAE-W, and the Q factor for the CAE-R due to conductor losses for TEM, TE, and TM modes. We provide normalized attenuation and Q-factor charts to assist microwave designers who need to estimate the practical utility of these structures. Besides this, we compare the attenuations charts for CAE-Ws and CAE-Rs with respect to corresponding charts for coaxial waveguides and resonators. These comparisons can help in the study of coaxial waveguides that are deformed to elliptic waveguides by applying an external perturbation, e.g., pressure.

II. LOSSES DUE TO CONDUCTING WALLS

The CAE geometry is shown in Fig. 1, where the elliptic coordinates are defined. The inner and outer walls correspond to curves ξ_1 = constant and ξ_2 = constant, and they have a sufficiently high-conductivity σ to be considered as good conductors. The intervening space is completely filled by a homogeneous lossy dielectric with permittivity $\epsilon_d = \epsilon' - j\epsilon''$, and free-space permeability μ. In particular, for a CAE-R, the end-plates are at $z = 0$, and $z = L$. We assume the usual $\exp[j\omega t - (\alpha + j\beta)z]$ dependence for traveling waves in a constant cross-sectional structure.

The formal solution for the traveling modes of CAE-Ws and resonant modes of CAE-Rs under lossless condition can be found in the literature [5]–[7]. The analytical expressions of the fields are written in terms of radial $[_eR(\xi) = Ce_m(\xi, q) + F_m Fey_m(\xi, q)]$ and angular $[ce_m(\eta, q)]$ even Mathieu functions, where F_m is a constant and $q = q_{r,m}$ is the rth eigenvalue of the characteristic equation corresponding to the Dirichlet or Neumann condition of the electric field at the walls. In the same manner, the odd solutions are written as $[_oR(\xi) = Se_m(\xi, q) + G_m Gey_m(\xi, q)]$ and $[se_m(\eta, q)]$.

A. Attenuation Constant for CAE-Ws

According to the first-order perturbation method [14], the attenuation constant α (Np/m) for a given propagating mode (r, m) is written as $\alpha = P_L/2P_T$, where P_L is the per-unit length power loss, and P_T is the power flowing through the waveguide. On the other hand, the Q factor for a given resonant mode (r, m, p) is given by $Q = \omega^{\mathrm{res}} U/P$, where U is the energy stored in the resonator, and P is the average power loss. Evaluating α and the Q factor due to losses in imperfect dielectric yields the same results for a cylindrical structure of any cross section [14]. Therefore, we shall restrict ourselves to calculate the losses due to finite conductivity of the elliptic walls.

The conducting losses are calculated by involving the inner and outer conductors, where we have applied a constant surface impedance $R_w = \sqrt{\omega\mu/2\sigma}$ in each point of the surfaces. The normalized attenuation constants are given by

$$\alpha_{\mathrm{TEM}}\sqrt{\sigma Z\rho^3} = \frac{\sqrt{V}}{\sqrt{2}\pi}\left[\frac{e_1 K(e_1^2) + e_2 K(e_2^2)}{\xi_2 - \xi_1}\right] \tag{1}$$

$$\alpha_{\mathrm{TE}}\sqrt{\sigma Z\rho^3} = \frac{q^{1/4}}{2I_4}\left[\frac{4qA}{\sqrt{W^3 - W}} + B\sqrt{\frac{W^2 - 1}{W}}\right] \tag{2}$$

$$\alpha_{\mathrm{TM}}\sqrt{\sigma Z\rho^3} = \frac{q^{1/4}C}{2I_4}\sqrt{\frac{W^3}{W^2 - 1}} \tag{3}$$

where $Z = \sqrt{\mu/\epsilon'}$ is the intrinsic impedance, $V \equiv \rho k = \sqrt{\mu\epsilon'}\rho\omega$, the eccentricities are written as $e_i = 1/\cosh(\xi_i)$, $K(e_i^2) = \int_0^{\pi/2} d\eta \left(1 - e_i^2 \sin^2\eta\right)^{-1/2}$ is the complete elliptic integral of the first kind, W is the normalized angular frequency

$$W \equiv \frac{\omega}{\omega^{\mathrm{cutoff}}} = \frac{\omega}{(\rho\sqrt{\mu\epsilon'})^{-1}\sqrt{4q}} = \frac{V}{\sqrt{4q}} \geq 1 \tag{4}$$

and

$$A \equiv R^2(\xi_1)I_{11} + R^2(\xi_2)I_{12}$$
$$B \equiv R^2(\xi_1)I_{21} + R^2(\xi_2)I_{22}$$
$$C \equiv R'^2(\xi_1)I_{31} + R'^2(\xi_2)I_{32}.$$

The integrals $I_{j,i}$ are given by the following expressions for each $i = \{1, 2\}$:

$$I_{1i} = \int_0^{2\pi} ce^2(\eta)\sqrt{\cosh^2\xi_i - \cos^2\eta}\, d\eta \tag{5a}$$

$$I_{2i} = \int_0^{2\pi} \frac{ce'^2(\eta)}{\sqrt{\cosh^2\xi_i - \cos^2\eta}}\, d\eta \tag{5b}$$

$$I_{3i} = \int_0^{2\pi} \frac{ce^2(\eta)}{\sqrt{\cosh^2\xi_i - \cos^2\eta}}\, d\eta \tag{5c}$$

$$I_4 = \int_{\xi_1}^{\xi_2} \int_0^{2\pi} \left[R'^2(\xi)ce^2(\eta) + R^2(\xi)ce'^2(\eta)\right]d\eta\, d\xi. \tag{5d}$$

The prime denotes the first derivative with respect to the argument ξ or η, as the case may be. The attenuation constants for odd modes are calculated by replacing the even parameters and Mathieu functions in the above equations by its corresponding odd ones.

B. Q Factor for CAE-Rs

By following the standard procedure [14], we find that the normalized Q factors are given by

$$\frac{Q_{\mathrm{TEM}}}{\sqrt{2\sigma ZL}} = \frac{\pi\sqrt{p\pi}}{4\Lambda}\left(\frac{\xi_2 - \xi_1}{e_1 K(e_1^2) + e_2 K(e_2^2)}\right) \tag{6}$$

$$\frac{Q_{\mathrm{TE}}}{\sqrt{2\sigma ZL}} = \left[16q\Lambda^2 + p^2\pi^2\right]^{1/4}$$
$$\cdot \frac{64q^2 I_5\Lambda^2 + p^2\pi^2 I_4}{128q^2 A\Lambda^3 + 2p^2\pi^2 B\Lambda + 4p^2\pi^2 I_4} \tag{7}$$

$$\frac{Q_{\mathrm{TM}}}{\sqrt{2\sigma ZL}} = \left[16q\Lambda^2 + p^2\pi^2\right]^{1/4}\frac{I_4}{2C\Lambda + 4I_4} \tag{8}$$

where $\Lambda \equiv L/2\rho$, I_4 is defined in (5d), and

$$I_5 = \int_{\xi_1}^{\xi_2} \int_0^{2\pi} R^2(\xi)ce^2(\eta)\left[\cosh^2\xi - \cos^2\eta\right]d\eta\, d\xi.$$

III. ATTENUATION CHARTS FOR CAE-Ws

From (1), it is evident that the attenuation for TEM modes depends on the square root of the frequency. Once the dimensions of the guide have been determined, α is calculated by evaluating the elliptic integrals, which are tabulated and plotted elsewhere [16]. Calculating the attenuation constant for TE and TM modes is a more complicated task because it implies the evaluation of integrals involving the Mathieu functions and its derivatives.

In order to plot the attenuation constants for the higher modes, we see that the right-hand side of (2) and (3) are function of the dimensionless parameter $V \equiv \sqrt{\mu\epsilon'}\rho\omega$, and the remaining quantities depend exclusively on ξ_1 and ξ_2. This fact permits us to plot for each mode a single chart for any combination of the eccentricities. We have applied a Newton–Cotes high-order method to evaluate the single integrals I_{qi}, and we have taken advantage of the separability of I_4 and I_5 to split them into single integrals. We have used the Bessel function product series for evaluating the radial Mathieu functions of the first and second kinds, and the usual Fourier series for angular Mathieu functions [15]–[17]. The results of our numerical routines for computing Mathieu functions have been compared with respect to results from recent publications [18], [19] and an accuracy of 10^{-9} was obtained. The routines also have been used to reproduce the sequence of eigenvalues in an elliptic waveguide, showing an excellent agreement with the values reported in the literature [20], [21].

Curves of normalized attenuation constants for the lower modes are given in Figs. 2–4. We include in each curve the
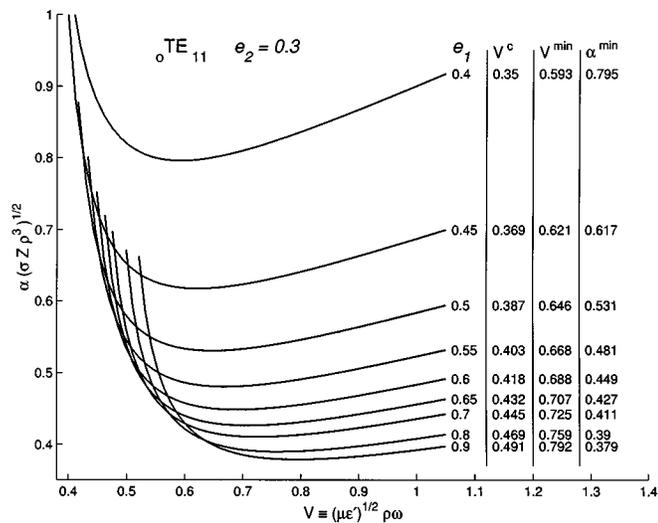
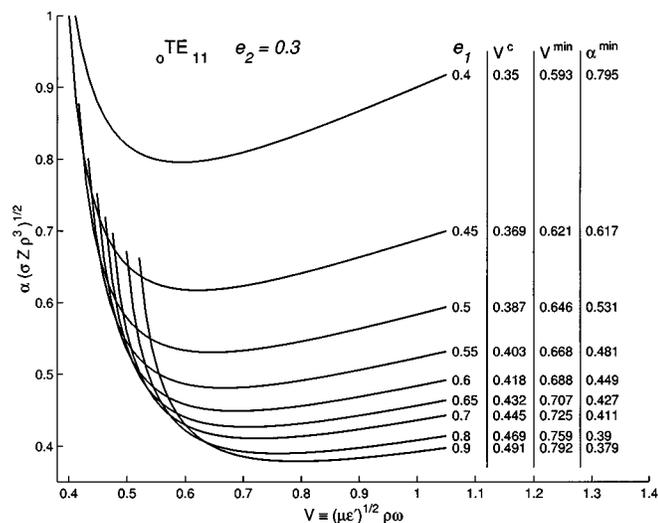Fig. 2. Normalized attenuation charts for $_o\text{TE}_{11}$ with $e_2 = 0.3$.

Fig. 4. Normalized attenuation charts for $_e\text{TM}_{01}$ with $e_2 = 0.3$.

Fig. 3. Normalized attenuation charts for $_e\text{TE}_{11}$ with $e_2 = 0.3$.

numerical values of the normalized cutoff frequency V^c, the frequency corresponding to minimum attenuation $V^{\min}$, and minimum attenuation $\alpha^{\min}$.

Comparison of V^c in Figs. 2–4 for the same values of e_1 and e_2 shows that $_o\text{TE}_{11}$ becomes the first higher mode for CAE-Ws. A physical explanation of this result is that the energy in even modes has a tendency to vibrate along the x-axis of the ellipse, whereas the odd modes do it along the y-axis. This fact leads to $_e\omega^c < {}_o\omega^c$ and $_e\text{TE}_{11}$ to be the fundamental mode in *hollow* elliptic waveguides [9], [20], [22]. However, in the confocal *annular* geometry, the inner conductor changes the relative distances (see Fig. 1) such that now the vertical separation b' becomes larger than the horizontal separation a'. From Fig. 1, it is straightforward to prove that

$$b' - a' = \frac{\rho}{2}\left[\exp(-\xi_1) - \exp(-\xi_2)\right] > 0$$

for any $\xi_2 > \xi_1 > 0$. As a consequence of this result, the even modes vibrate in shorter distances than odd modes and, thus, the cutoff frequency of the odd modes becomes smaller than
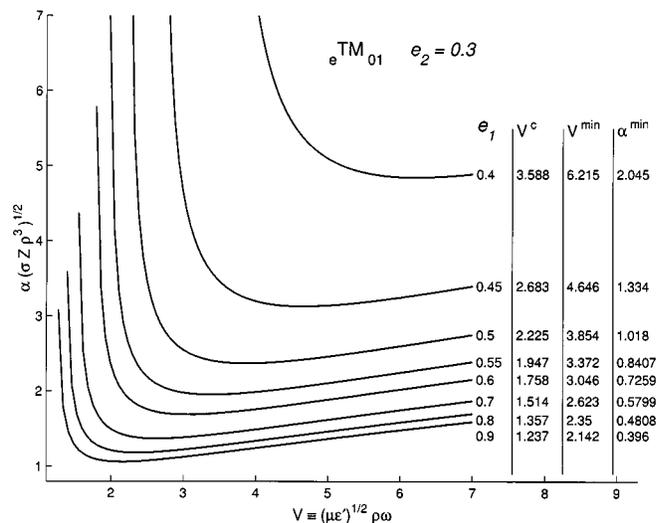
the cutoff frequency in even modes. On the other hand, for the same values of e_1 and e_2, the cutoff frequency for TM modes is notably larger than TE modes.

From Figs. 2 and 3, it is clear that the attenuation for dominant mode $_o\text{TE}_{11}$ is slightly larger than the attenuation of the even $_e\text{TE}_{11}$ for the same value of frequency and eccentricities. However, TE_{11} modes behave differently, as seen in Fig. 4.
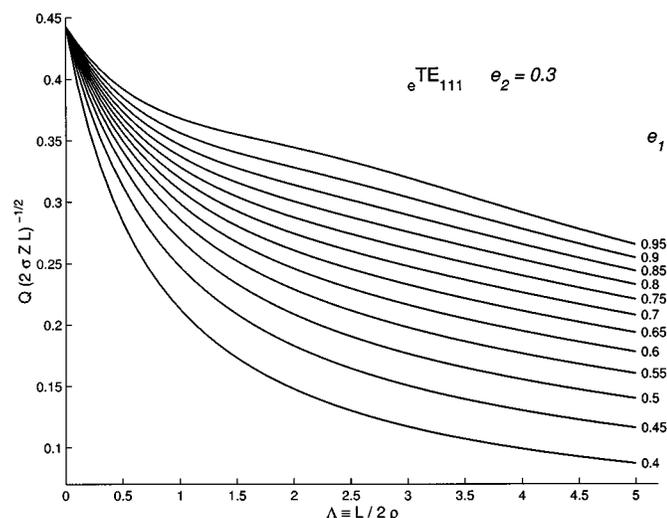
For each combination of e_1 and e_2, there is a frequency range where the modes have the lowest attenuation. The value of $V^{\min}$ is determined by differentiating, with respect to W, (2) and (3), and equating to zero. For TE modes, we obtain

$$W^{10} - W^8 - (2 + 9G)W^6 + (2 + 15G)W^4$$
$$+ (1 - 7G)W^2 + G - 1 = 0$$

where $G \equiv (4qA/B)^2$. The only real root larger than unity of this even-polynomial corresponds to the minimum W, and it is related to $V^{\min}$ by (4). From the data of Figs. 2 and 3, we can see that $V^{\min}$ is approximately 150%–170% greater than V^c. In the same manner, for TM modes, we obtain the exact and remarkable result $W^{\min} = \sqrt{3}$, which leads to $V^{\min} = \sqrt{3}V^c$, as can be observed in Fig. 4. From the attenuation charts, it is evident that, at a given frequency and focal separation distance, the attenuation increases as the eccentricities get closer.

If we change e_1 by maintaining constant e_2, the cutoff frequencies of the TE modes behave differently than the cutoff frequencies of the TM modes. In charts for TE modes (Figs. 2 and 3), we see that V^c increases as e_1 increases, whereas for TM modes (Fig. 4), V^c decreases as e_1 increases. In both cases, the change of V^c occurs more slowly as e_1 becomes larger.

It must be mentioned that the attenuation charts for CAE-Ws do not tend to charts for hollow elliptic waveguides [10] as $e_1 \to 1$ (i.e., $\xi_1 \to 0$). The reason for this is that the boundary condition at ξ_1 is maintained when $\xi_1 \to 0$ (similar to a thin conducting sheet joining the foci along the waveguide, Fig. 1), and it is obviously a condition not present in hollow waveguides. However, when the focal separation tends to zero, we recover the coaxial waveguide charts.
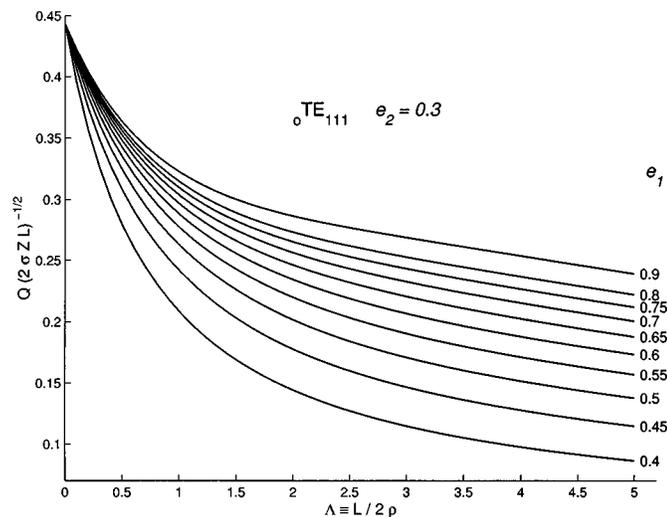
Fig. 5. Normalized Q-factor charts for $_o\mathrm{TE}_{111}$ with $e_2 = 0.3$.
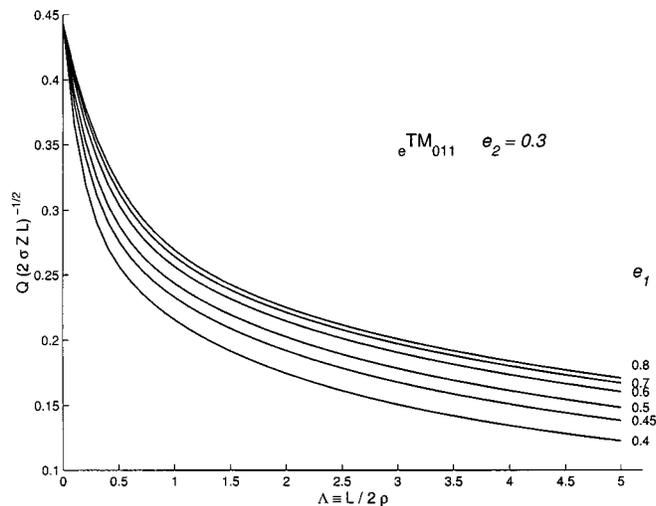
Fig. 7. Normalized Q-factor charts for $_e\mathrm{TM}_{011}$ with $e_2 = 0.3$.

Fig. 6. Normalized Q-factor charts for $_e\mathrm{TE}_{111}$ with $e_2 = 0.3$.

Fig. 8. Attenuation charts for TE_{11} in a CG and $_o\mathrm{TE}_{11}$ in a CAE-W, with the same cutoff frequency and cross-sectional area.
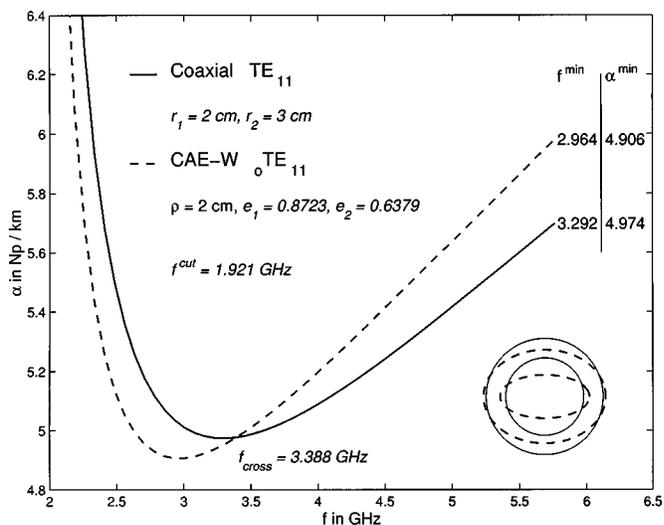
IV. Q-FACTOR CHARTS FOR CAE-Rs

In Figs. 5–7, we include charts of the normalized Q factor in function of dimensionless parameter $\Lambda \equiv L/2\rho$. The resonant frequencies for TE or TM modes in the resonator are given by [7]

$$f_{r,m,p}^{\mathrm{res}} = \frac{1}{2\pi\sqrt{\mu\epsilon}} \sqrt{\frac{4q_{r,m}}{\rho^2} + \frac{p^2\pi^2}{L^2}}. \qquad (9)$$

From (9) and data of cutoff frequencies in Figs. 2–4, it is clear that $_of_{111}^{\mathrm{res}}$ and $_ef_{010}^{\mathrm{res}}$ become the fundamental resonant frequencies for TE and TM modes, respectively. In particular, for TM modes, the substitution $p = 0$ in (9) leads to $f_{r,m,0}^{\mathrm{res}} = f_{r,m}^{\mathrm{cut}}$, and the resonant frequencies coincide with cutoff frequencies of the equivalent waveguide. Since the results of the perturbation method are valid for frequencies not so close to the cutoff condition, the charts corresponding to $p = 0$ are not included.

Similar to CAE-Ws, for the same value of the eccentricities, the presence of the inner conductor in the CAE-R leads to $_of_{r,m,p}^{\mathrm{res}} < {_ef_{r,m,p}^{\mathrm{res}}}$ for TE and TM modes. From (7) and

(8), as $\Lambda \to 0$, the value of Q for TE and TM modes tends to $\sqrt{\sigma p \pi Z L/8}$, and besides, this limit is equal for the coaxial resonator (CR) when the same normalization is applied. However, at a given $\Lambda > 0$, the Q-factor for $\mathrm{TE}_{r,m,p}$ modes becomes greater than Q for $\mathrm{TM}_{r,m,p}$ modes. By comparing Figs. 5 and 6, we observe that Q in even-TE modes is larger than Q in odd-TE modes, similarly, Q in odd-TM modes is greater than Q in even-TM modes. At a given Λ, the Q factor decreases as the eccentricities get closer, and this occurs more rapidly as the eccentricities become smaller.

V. COMPARISON BETWEEN CAE-Ws AND CAE-Rs WITH COAXIAL GUIDES AND RESONATORS

In Fig. 8, we show the attenuation charts for the first higher mode TE_{11} in a copper air-filled coaxial guide (CG), and for the highest mode, $_o\mathrm{TE}_{11}$ in a copper air-filled CAE-W. In order to make appropriate comparisons, both guides have the same cutoff frequency and cross-sectional propagating area. The expressions for the attenuation due to conducting walls in
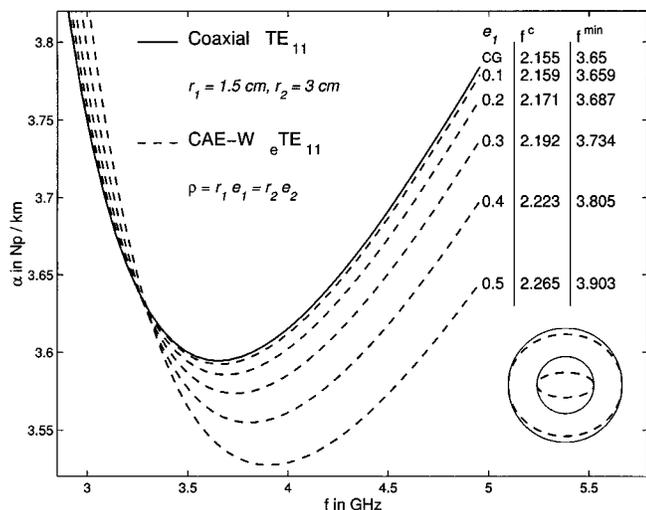
Fig. 9. Attenuation charts for TE_{11} in a CG and $_eTE_{11}$ in a CAE-W for different eccentricities, but the same largest axes.
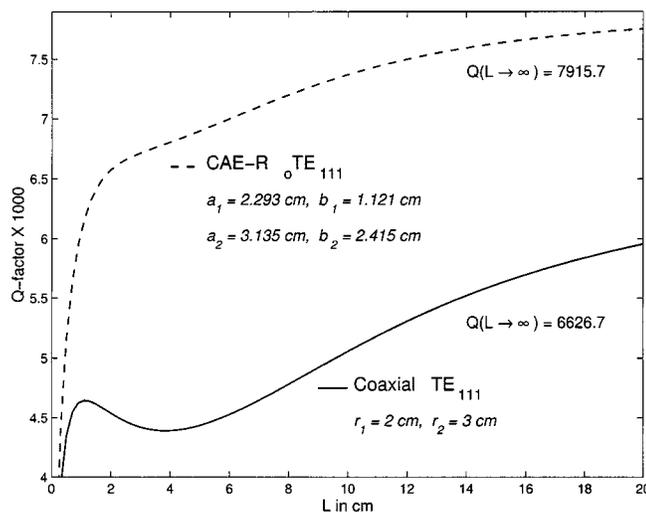

Fig. 10. Q-factor chart for TE_{111} in a CR and $_oTE_{111}$ in a CAE-R, with the same resonant frequency and volume as L increases. Note that Q-axis scale starts at 4000.

a CG can be found in [14]. The dimensions, cutoff frequency, and minima attenuations for both guides are included. From Fig. 8, we see that, closer to f^{cut}, the CAE-W has lower α than the CG, but at higher frequencies, the attenuation in CAE-Ws increases more rapidly than the attenuation in the CG. It is interesting to see that there exists a frequency f^{cross} where both guides have the same attenuation. This intersection frequency can be calculated by equating the attenuation constants for the CG and CAE-W, but unfortunately, the complexity of (2) impedes to obtain a closed-form expression, and f^{cross} must be evaluated by finding the roots of a transcendental equation.

In Fig. 9, we compare the attenuation curves in a CAE-W as its geometry tends to a CG. Contrary to the previous example, here we change the eccentricities and focal distance in each curve such that the largest axes of the ellipses maintain always the same value as the radii of the CG. We can see that attenuation increases and cutoff decreases as the CAE-W becomes more circular. With $e_1 = 0.1$, the shorter axis of the ellipse is

0.5% smaller than the largest axis, and the curves get very close. Similar to the above example, the curves intersect at a specific frequency f^{cross}. The CAE-W presents a lower attenuation than the CG in the neighborhood around a minimum of α.

Finally, a comparative chart between the Q factor of the TE_{111} mode in a CR and the $_oTE_{111}$ mode in a CAE-R is given in Fig. 10. In order to have the same resonant frequency and volume in both resonators as L increases, we select the size of the cross sections and the physical quantities equal to the example of Fig. 8. One result of this comparison is that the Q factor in a CAE-R is 20%–40% greater than the Q factor for CR if both resonators operate in their first higher mode. By making $L \to \infty$ in (7) and (8), the upper limits of Q for TE and TM modes are given by $Q_{TE} = 2q^{1/4}I_5\sqrt{\sigma Z\rho}/A$, and $Q_{TM} = 2q^{1/4}I_4\sqrt{\sigma Z\rho}/C$.

VI. CONCLUSIONS

The first-order perturbation method has been used to calculate the attenuation and Q-factor parameters due to conducting losses in CAE-Ws and CAE-Rs. An important consequence of incorporating the inner elliptic conductor is that the odd modes become more dominant than even modes, in particular, the mode $_oTE_{11}$ becomes the first higher mode in CAE-Ws. Normalization of the attenuation constant and Q factor makes it possible to present for each mode a single chart for all possible combinations of frequencies, eccentricities, focal separation distances, and conductivities. It was found that the attenuation increases and the Q factor decreases as the eccentricities of the conductors get closer, and this occurs more rapidly as the eccentricities becomes smaller. Appropriate comparisons between CAE-Ws and CGs exhibit the lower cutoff frequency and attenuation for the elliptic geometry. In the same manner, it was found that CAE-Rs present a larger Q factor than a CR with the same volume if both work in their first higher mode. A supplement to this paper, including the lossless solutions and additional figures, can be found online.[1]

REFERENCES

[1] A. K. Bhattacharyya and L. Shafai, "Theoretical and experimental investigation of the elliptical annual ring antenna," *IEEE Trans. Antennas Propagat.*, vol. 36, pp. 1526–1530, Nov. 1988.
[2] Y. Hu, F. M. Ghannouchi, and R. G. Bosisio, "Theoretical and experimental measurement of microwave permittivity using open ended elliptical coaxial probes," *IEEE Trans. Microwave Theory Tech.*, vol. 40, pp. 143–150, Jan. 1992.
[3] K. Sun and J. M. Tranquilla, "Study of elliptical annular microstrip antenna using full Mathieu formulation," in *IEEE Int. AP-S Symp. Dig.*, vol. 2, 1994, pp. 944–947.
[4] F. A. Alhargan and S. R. Judah, "Wide-band confocal annular elliptic microstrip antenna," in *IEEE Int. AP-S Symp. Dig.*, vol. 2, 1995, pp. 1006–1009.
[5] M. J. King and J. C. Wiltse, "Coaxial transmission lines of elliptical cross section," *IRE Trans. Antennas Propagat.*, vol. AP-9, pp. 116–118, Jan. 1961.
[6] F. A. Alhargan and S. R. Judah, "Mode charts for confocal annular elliptic resonators," *Proc. Inst. Elect. Eng.*, pt. H, vol. 143, pp. 358–360, Aug. 1996.
[7] K. Hong and J. Kim, "Natural mode analysis of hollow and annular elliptical cylindrical cavities," *J. Sound Vib.*, vol. 183, no. 2, pp. 327–351, 1995.

[1][Online]. Available: http://homepages.mty.itesm.mx/jgutierr/CAE.htm

[8] R. Navarro, V. E. Boria, B. Gimeno, A. Coves, and M. Ferrando, "Full modal analysis of confocal coaxial elliptical waveguides," *Proc. Inst. Elect. Eng.*, pt. H, vol. 147, no. 5, pp. 374–380, Oct. 2000.

[9] L. J. Chu, "Electromagnetic waves in elliptic hollow pipes of metal," *J. Appl. Phys.*, vol. 9, no. 9, pp. 583–591, Sept. 1938.

[10] J. G. Kretzschmar, "Attenuation characteristics of hollow conducting elliptical waveguides," *IEEE Trans. Microwave Theory Tech.*, vol. MTT-20, pp. 280–284, Apr. 1972.

[11] G. Falciasecca, C. G. Someda, and F. Valdoni, "Comments on 'Attenuation characteristics of hollow conducting elliptical waveguides'," *IEEE Trans. Microwave Theory Tech.*, vol. MTT-21, p. 154, Mar. 1973.

[12] L. Lewin and A. M. B. Al-Hariri, "The effect of cross-section curvature on attenuation in elliptic waveguides and a basic correction to previous formula," *IEEE Trans. Microwave Theory Tech.*, vol. MTT-22, pp. 504–509, June 1974.

[13] S. R. Rengarajan and J. E. Lewin, "Surface impedance of elliptical hollow conducting waveguides," *Electron. Lett.*, vol. 15, no. 20, pp. 637–639, Sept. 1979.

[14] G. F. Miner, *Lines and Electromagnetic Fields for Engineers*. Oxford, U.K.: Oxford Univ. Press, 1996.

[15] N. W. McLachlan, *Theory and Application of Mathieu Functions*. Oxford, U.K.: Oxford Univ. Press, 1951.

[16] M. Abramowitz and I. Stegun, *Handbook of Mathematical Functions*. New York: Dover, 1964.

[17] I. S. Gradshteyn and I. M. Ryzhik, *Table of Integrals, Series, and Products*, 5th ed. New York: Academic, 1994.

[18] R. Shirts, "Algorithm 721 MTIEU1 and MTIEU2: Two subroutines to compute eigenvalues and solutions to Mathieu's differential equation for noninteger and integer order," *ACM Trans. Math. Softw.*, vol. 19, no. 3, pp. 397–406, Sept. 1993.

[19] F. A. Alhargan, "A complete method for the computation of Mathieu characteristics numbers of integer orders," *SIAM Rev.*, vol. 38, no. 2, pp. 239–255, June 1996.

[20] S. Zhang and Y. Shen, "Eigenmode sequence for an elliptical waveguide with arbitrary ellipticity," *IEEE Trans. Microwave Theory Tech.*, vol. 43, pp. 227–230, Jan. 1995.

[21] M. Schneider and J. Marquardt, "Fast computation of modified Mathieu functions applied to elliptical waveguide problems," *IEEE Trans. Microwave Theory Tech.*, vol. 47, pp. 513–516, Apr. 1999.

[22] J. G. Kretzschmar, "Wave propagation in hollow conducting elliptical waveguides," *IEEE Trans. Microwave Theory Tech.*, vol. MTT-18, pp. 547–554, Sept. 1970.

Julio C. Gutiérrez-Vega received the B.S. degree in physics and M.S. degree in electric engineering from the Instituto Tecnológico y de Estudios Superiores de Monterrey (ITESM), Monterrey, México, in 1991 and 1995, respectively, and the Ph.D. degree in optics from the Instituto Nacional de Astrofísica, Optica y Electrónica (INAOE), Puebla, México, in 2000.

In 1992, he joined the Center of Optics, ITESM, where he was involved in the design of fiber-optics sensors and optical waveguides. He is currently with the Physics Department, ITESM. His research interest includes mode analysis of laser and microwave cavities, wave propagation of invariant optical fields, and electrooptics.

Dr. Gutiérrez-Vega is a member of the Optical Society of America (OSA) and Mexican Optical Society.

Ramón M. Rodríguez-Dagnino (S'89–M'91) received the Ph.D. degree from the University of Toronto, Toronto, ON, Canada, in 1993, the M.Sc. degree from the Research and Advanced Studios Center (CInvEstAv), México City, México, in 1984, all in electrical engineering.

From 1984 to 1989, he was with the Research and Development Center, Telmex (a Mexican telephone company). Since 1993, he has been a Full-Time Professor with the Center for Electronics and Telecommunications, Instituto Tecnológico y de Estudios Superiores de Monterrey (ITESM), Monterrey, México. From 2000–2001, he was the Director of the Electronics and Telecommunications Center, ITESM. His current research interest includes electromagnetics, teletraffic modeling, multimedia network design, and communication theory.

Dr. Rodríguez-Dagnino is a member of the Mexican National System of Research (SNI). He has served as a technical reviewer of several IEEE journals and conferences and has been a committee member of SPIE conferences.

Sabino Chávez-Cerda received the B.Sc. degree in physics from the Escuela Superior de Fisica y Matematicas, Instituto Politécnico Nacional (IPN), México City, México, in 1988, the M.Sc. degree in optics from the Centro de Investigaciones en Optica, León, México, in 1990, and the Ph.D. degree in optics from the Imperial College, London, U.K., in 1994.

He is currently a Researcher in the Optics Division, Instituto Nacional de Astrofísica, Optica y Electrónica (INAOE), Puebla, México. His research interest includes optical pulse and beam propagation in linear and nonlinear media, and optical solitons.

Dr. Chávez-Chávez is a Chartered Physicist of the Institute of Physics (IOP). He is a member of the Optical Society of America (OSA) and Mexican Optical Society.